Journal of Asian Earth Sciences 62 (2013) 317–328

Contents lists available at SciVerse ScienceDirect

Journal of Asian Earth Sciences

journal homepage: www.elsevier.com/locate/jseaes

Arshan palaeoseismic feature of the Tunka fault (Baikal rift zone, Russia)

Oleg P. Smekalin [a], Alexander A. Shchetnikov [a,*], Dustin White [b]

[a] Institute of the Earth's Crust, Siberian Branch of the Russian Academy of Sciences, Lermontov Street 128, Irkutsk 664033, Russia
[b] Archaeology, University of Southampton, Avenue Campus, Southampton SO17 1BF, United Kingdom

ARTICLE INFO

Article history:
Received 4 January 2012
Received in revised form 4 October 2012
Accepted 8 October 2012
Available online 23 October 2012

Keywords:
Palaeoseismic features
Baikal rift zone
Siberia

ABSTRACT

The traditional concept of the rift development of flank depressions in the Baikal rift zone is now doubted in view of some indicators for compression deformations identified by the seismogeological and geodetic methods. Besides, the paleoseismological investigations revealed seismogenic strike-slips and reverse faults in the Tunka fault zone that is a major structure-controlling element of the Tunka rift depression. However, a detailed study of the upslope-facing scarp in the Arshan paleoseismogenic structure zone has shown that its formation might be due to rift mechanism of basin formation. Age estimation has been made for the previously unknown pre-historic earthquake whose epicentral area coincides with the western flank of the Arshan paleoseismogenic structure. Judging from previously determined ages of paleoearthquakes, the mean recurrence period for faulting events on the central Tunka fault is 2780–3440 years.

1. Introduction

The Tunka depression consists of six different-sized basins separated by basement uplifts on the southwestern flank of the Baikal rift zone (Fig 1). Early geological investigations (Florensov, 1960, 1969; Zorin, 1972; Solonenko, 1975) showed that the Tunka depression is similar in geological-tectonic structure and developmental history to the inland basins of the central and northeastern branches of the Baikal rift. Abundant evidence obtained from a decade-long, comprehensive study of rift basins and basin-bordering mountains, indicates a complicated mechanism of interaction between rifting and formation of domal horst structures covering an area considerably larger than the Tunka rift. The development of rift basins occurs in the context of a general uplift of the area south of the Siberian platform, including the mountains bordering it on the south (Sharyzhalgai ridge, Baikal dome and others), with an absolute subsidence related only to the proper Tunka basin. Another five satellite basins have undergone only relative subsidence, i.e. the basin bottoms, when uplifting, do not keep pace with the basin-bordering hilltop and base surfaces in growth. The marginal flank basins – Mondy and Bystrinsky (13 and 14 in Fig. 2) – have already ceased to be areas of sedimentation and become the elements of inner structure of inversion blocks of inter-rift mountain ridges. The bottoms of these basins are tectonically deformed. The previously existing sedimentation surfaces are distorted, broken into steps, and intensively eroded.

The inversion uplifts also involve large areas of major rift basins (Khoitogol, Tunka, Tora) (labels 7, 10, and 12 in Fig. 2). Most of these areas are adjacent to crystalline interbasin uplifts and the bottom part of the intense domal uplift of the Khamar-Daban ridge. At present, about 40% of the Tunka basin area has ceased to be the scene of sedimentation (Shchetnikov, 2009; Shchetnikov et al., 2012).

The northern sides of the Tunka and Tora basins are controlled by the Tunka fault zone, whose eastern flank lies within the Tora basin and Elovsky ridge. Paleoseismic investigations (Chipizubov et al., 2003) have shown seismogenic deformations of the reverse-scarp type that were produced by numerous reverse slips. Seismotectonic deformations that are exactly the opposite of typically rifting deformations, i.e. with near-horizontal compression and extension axis normal to the earth surface, are characteristic of some $M > 4$ earthquake focal mechanisms (Fig. 2). Strike-slip deformations along the Tunka fault are indirectly indicated by fractures in the crystalline basement rocks and sometimes by river bends. Linear NE-trending folds in sedimentary fill of basins (Florensov, 1960) may be also indicative of probable compressions.

The authors of this paper believe that the strike-slip motion on the eastern part of the Tunka fault may be related to the eastward motion of the Tora basin as a structure developing on the Precambrian basement of the Slyudyanka block, and consequently the fault is part of the southwestern (hanging) side of the Main Sayan fault. The eastern segment of the Tunka fault splits the northern margin of the Slyudyanka block forming a buffer zone (the Derbinsky block) for displacement amplitude distribution between two large tectonic elements of the crust – Siberian platform and its southern folded border. Longitudinal extension of the Tunka basin

* Corresponding author. Tel.: +7 914 915 7735 (O); fax: +7 359 242 6900.
E-mail address: shchet@crust.irk.ru (A.A. Shchetnikov).

1367-9120/$ - see front matter © 2012 Elsevier Ltd. All rights reserved.
http://dx.doi.org/10.1016/j.jseaes.2012.10.011

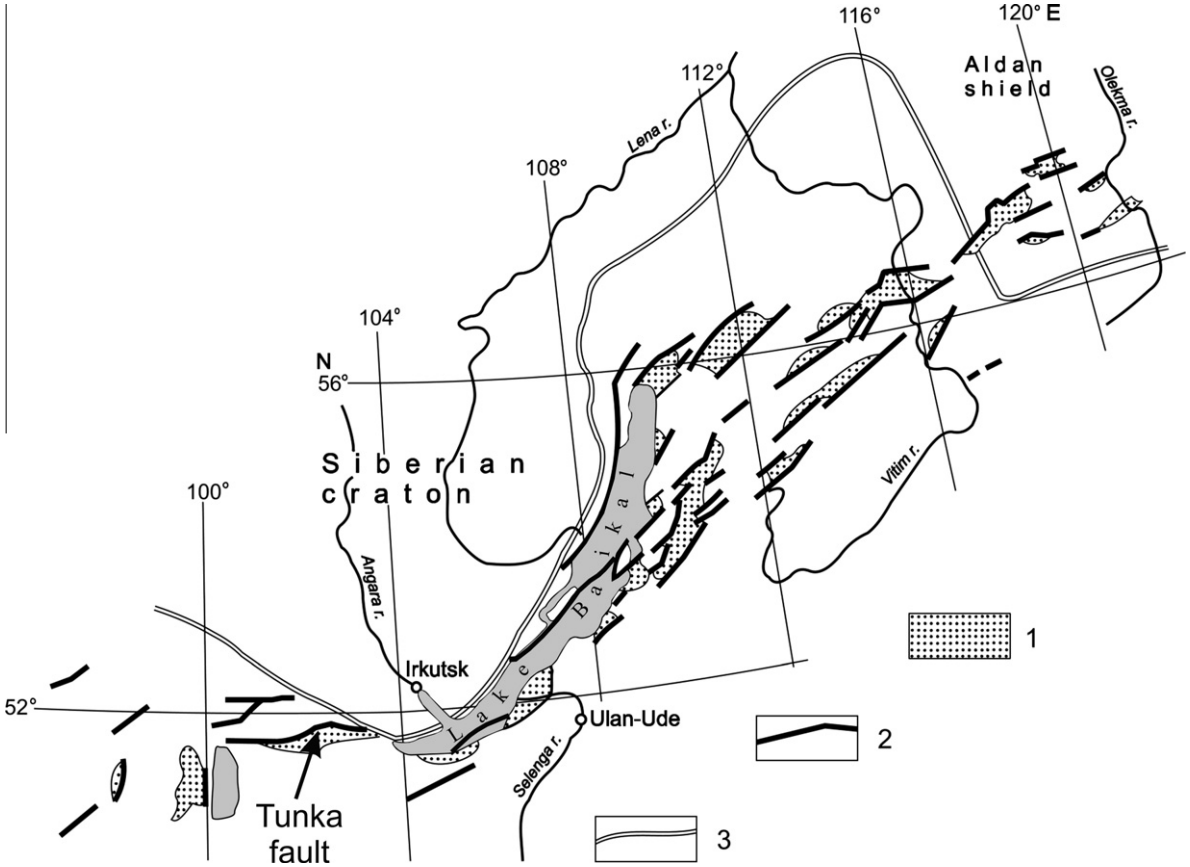

Fig. 1. Structural position and morphology of the Baikal rift system (after Logachev (2003)). 1 – rift basins, 2 – faults of various geometries, 3 – boundary between the Siberian craton and Sayan-Baikal orogenic belt.

predetermined its transverse divisibility to form basement uplifts between some basins, of which the most important is the proper Tunka basin whose northern side has been complicated by dislocations of the Arshan paleoseismogenic structure.

The Arshan structure was first described by seismogeologists from the Institute of the Earth's Crust of Siberian Branch of Russian Academy of Sciences (Solonenko et al., 1971; Solonenko, 1975), with an emphasis on normal-fault scarps and troughs as indications of paleoseismicity. Fault scarps formed by down-dip faulting of the Pleistocene terraces are 5–20 m high. The total height of the scarps is up to 50 m in the watershed areas, and testifies to a general effect of "several certain intensity earthquakes that took place over the last several hundred–first several thousand years". The troughs at the base of the scarp are up to 3–4 m deep and 10–70 m wide. Geomorphological research suggests that genetically the Arshan structure is "a fault with downthrown basin-bounding side, which follows the displacement along the major plane of the Tunka rift fault" (Florensov, 1969). The estimated intensity for the earthquake that produced the Arshan structure is at least equal to 10 points by the MSK-64 scale ($M > 7$).

Dislocations on the Arshan paleoseismogenic structure have a genetic link with near-horizontal extension, as evidenced by grabens at the bottom of fault scarps, cracks, and antithetic faults identified by geophysics. It is in this fault segment to which the Arshan structure is confined, that the gradient of vertical deformation attains its maximum as compared to other segments of the Tunka fault. Near the Arshan structure, there is evidence for the maximum downwarping of the basin basement. In this connection, the central segment of the Tunka fault can hardly be viewed as the site of even local reverse-fault type deformations, of the type that are common east of the basin border. However, within the Arshan structure the authors of this paper have found a 350-m long and ~5-m high reverse scarp whose existence is hard to explain in general geodynamic context of the southwestern Pribaikalye. The authors have attempted to solve this problem by a detailed study of the deformation in relation to the development of the Arshan dislocation as a whole.

2. Palaeoseismic features

Paleoearthquakes on the Arshan structure were first dated in the early 1990s (McCalpin and Khromovskikh, 1995). These results were obtained from C-14 dating of the samples collected in 1991 from buried soils in two quarry trench walls (A-6 – upper quarry exposure, A-7 – lower querry exposure), in a shallow trench near the seismic station (trench A-5 at the base of the normal fault bounding the 3rd terrace), and in a pit on the first terrace (AT-1). Note that trenches were excavated only in the central part of the structure, in the deposits on the alluvial fan terraces aligned parallel to the Kyngarga River (Fig. 3). For the present study we made three new excavations at variable distances west of the Kyngarga River. The revealed deformations in these new excavations provided new and stronger evidence in support of the paleoearthquakes identified by McCalpin and Khromovskikh (1995), and also identified a previously unknown paleoevent confined to the western flank of the Arshan structure.

This paper focuses on the development of Late Quaternary seismotectonic deformation processes on the segments of Tunka fault zone west of the Kyngarga River, which differ in the fault plane

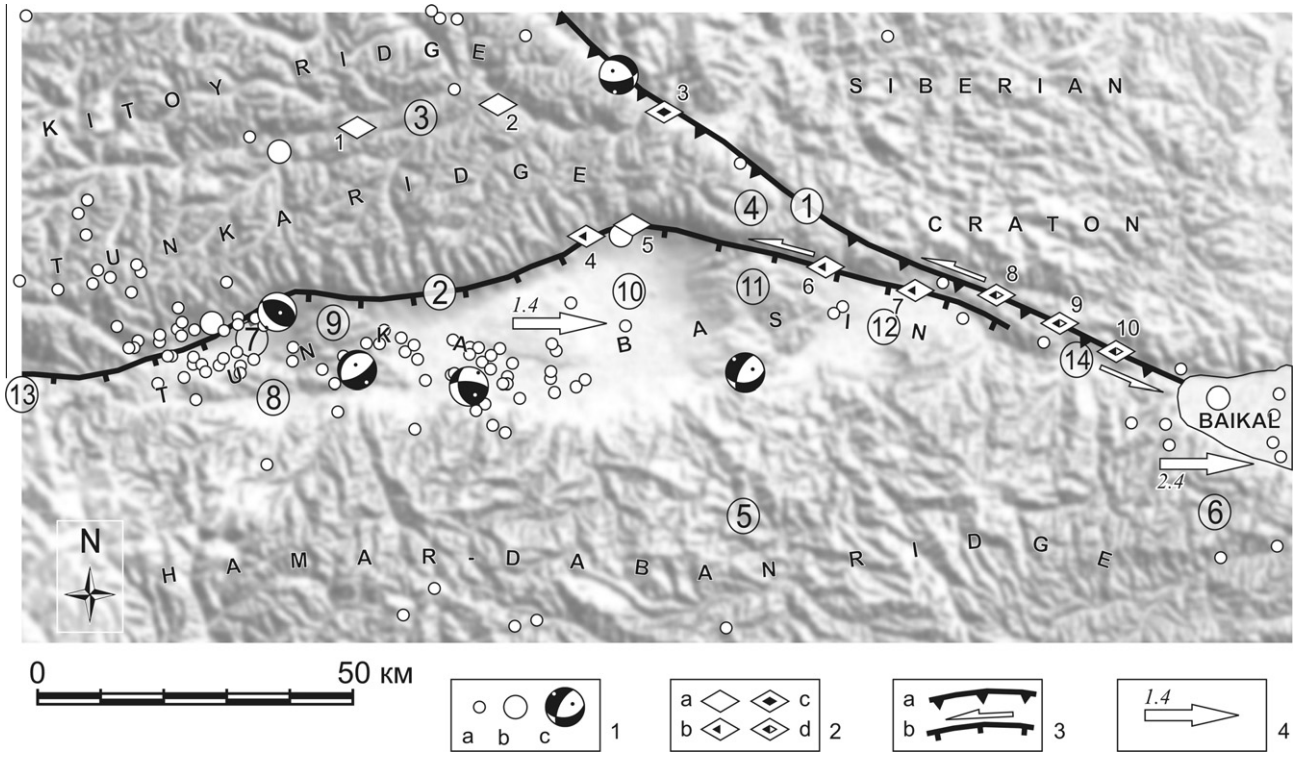

Fig. 2. A schematic view of seismicity and major structural elements of the southwestern Pribaikalye. Legend: 1 – recent seismicity (1950–2008): (a) epicenters of $3 < M < 5$ earthquakes, (b) epicenters of $M > 5$ earthquakes, (c) focal mechanisms (compression wave areas filled, principal axes of compression and tension stresses respectively shown by white and black dots, projections made for the lower hemisphere (Arzhannikova et al., 2007)); 2 – paleoseismogenic structures of the following genetic types: (a) normal fault, (b) left-lateral oblique-slip fault, (c) reverse fault, (d) left-lateral reverse slip. Numbers show the epicenters of paleoearthquakes within the following seismogenic structures: 1 – Kitoy, 2 – Shumak, 3 – Kitoy-Kinsky, 4, 5 – Arshan, 6, 7 – Tora, 8–10 – East Sayan; 3 – major faults: (a) reverse faults, (b) normal faults, hatches and triangles on the hanging side, arrows showing the directions of horizontal displacement component; 4 –horizontal velocity vector from GPS-geodetic measurements (1994–2002) relative to the Irkutsk GPS-site (San'kov et al., 2004). Circled numbers show the major structural elements of the southwestern Pribaikalye: 1 – Main Sayan fault, 2 – Tunka fault, 3 – Ilchir synclinorium (PR-PZ), 4 – Derbinsky block (AR), 5 – Khamar-Daban block (PR), 6 – Slyudyanka block (AR). Elements of the Tunka depression structure: 7 – Khoitogol basin, 8 – Turan basin, 9 – Nilovsky spur (interbasin high), 10 – Tunka basin, 11 – Elovsky spur, 12 – Tora basin, 13 – Mondy basin, 14 – Bystrinsky basin.

orientation and in type of motions from segments farther east. Our study was conducted in the western segment of dislocations of the Arshan seismogenic structure wherein the Buhota-Bugatai interfluve area is the juncture that connects fault segments striking northeast (west of the Bugatai River) with those of latitudinal strike (east of the Buhota River). This is one of the two extensive, strike-varying (about 40°) knee-shaped bends of the Tunka fault, which generally trends E–W.

The dislocations of the Arshan structure primarily include the 15 km long fault scarp extending from the Zun-Handagaiki River on the west to the Artemieva River on the east. The length of extension is based on arbitrarily proposed boundaries, since the flanks of the structure are still poorly known. Within these boundaries, the scarp is easily observed on large-scale aerial photographs. At the base of the scarp, there are graben-like troughs, linear landforms 30–250 m long each with either steep or gentle slopes. Some cross-section profiles (1, 13, 15, and 16 in Figs. 3 and 4) illustrate the morphology of the trough surface. The troughs at the base of a normal fault could result from near-surface branching of the fault that gives rise to antithetic faults trending toward the fault ridge. The antithetic faults border the walls of the graben-like troughs on the south and extend depthward merging with the main fault plane. These faults, parallel to the main normal fault, separate elongated structural blocks which extension-related subsidence exceeds than that of the downthrown side of the fault in general. Where the block subsidence is not compensated by sedimentation, the troughs can exist for a relatively long period. The described mechanism is characteristic of the formation of wide (10 m and wider) troughs with flat drainless bottoms. The sediment-filled graben at the base of the scarp on the west side of the Kyngarga River terrace complex (profile 1, Figs. 3 and 4) is complicated by a narrow deep trough that may be similar to the "crack"-type structures (McCalpin, 2005). These structures are sediment-filled cracks that occur when the fault plane shows a decrease in an angle of dip at some depth below the surface.

The deeper structure beneath the fault scarps has been interpreted from geoelectric sections. Six geophysical profiles were made along the western part of the structure, with three of these illustrated in Figs. 5 and 6. All geophysical profiles provided supporting evidence for faulting in both the sloping piedmont plain sediments and in solid rocks – crystalline slates and marmorized limestones. Profile 6 (Fig. 5), the only one measured where the fault strikes E–W, crosses the crack at the foot of the 4th terrace on the west side of Kyngarga River. The results clearly show a 45-m wide vertical-domain of low apparent resistivity, with the crack no wider than 12 m on the surface that indicates gradual divergence of the fault sides. The graben-shaped structure of dislocation has been acquired on the geophysical profiles, some of which were made in fault segments showing neither troughs nor sinkholes. The profile section interpretations for scarps with a NE strike show a consistent decrease in width of SW-trending low-velocity zones in the dislocation zone. They are scarcely a few meters wide (profile 5) near the Handagaika River (Fig. 3, west end of the general diagram).

The seismogenic scarp near the village of Arshan dissects complex alluvial fan-terrace deposits of the Kyngarga River. The main characteristics of the faulted terraces are summarized in Table 1.The amplitude of faulting at the second terrace, identified

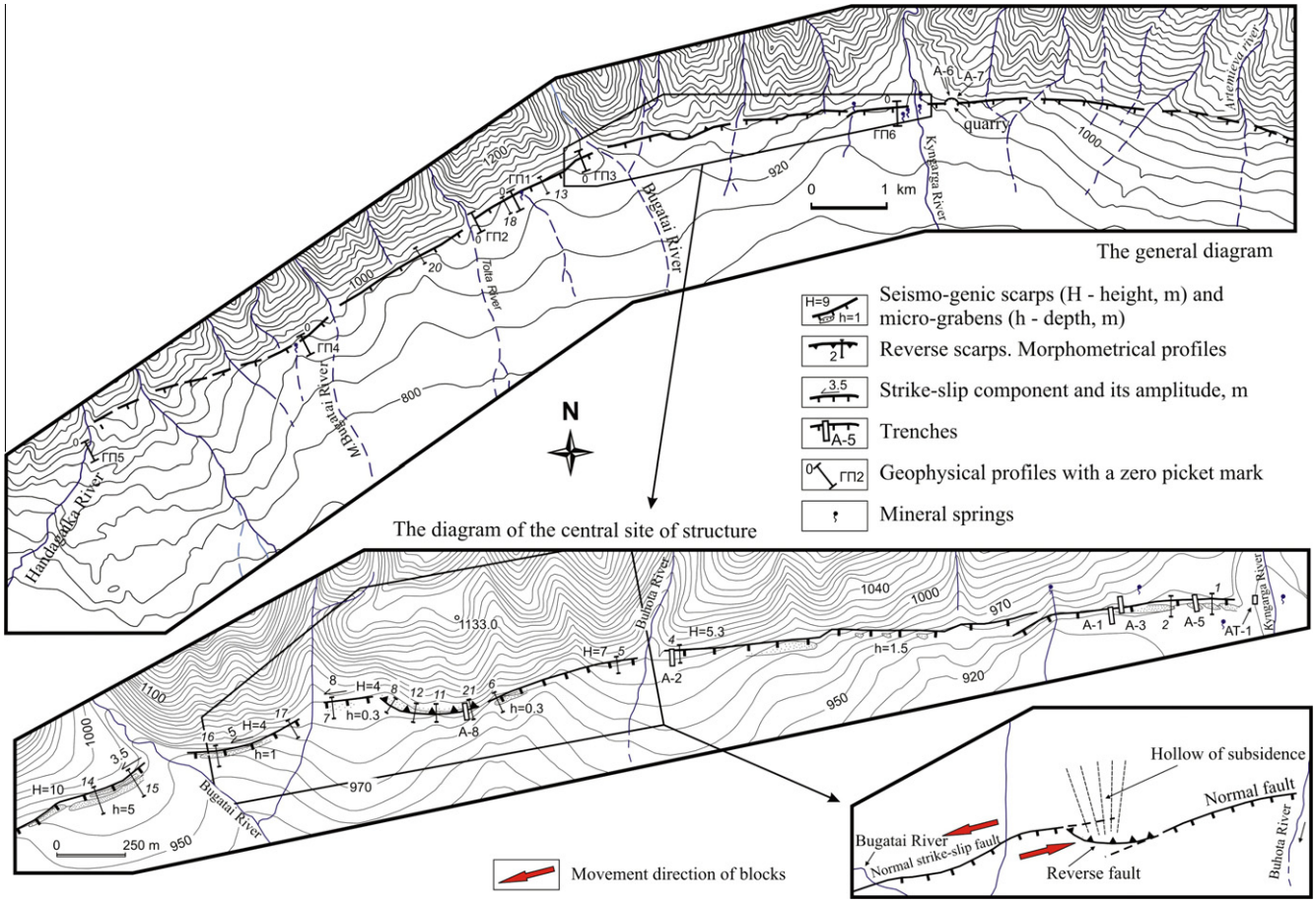

Fig. 3. Map of the central part of the Arshan seismogenic structure. The upper, general diagram shows an 18 km-long section from east of the Kyngarga River (village of Arshan), west to the Handagaiki River. The lower diagram of the central site is an enlargement of the 4.5 km-long section between the Kyngarga and Bugatai Rivers. Inset at lower right shows fault scarps in 1 1.5 km-long section between the Bugatai and Buhota Rivers.

with vertical displacements during the last paleoevent, is also a part of a 9 m scarp offsetting the third and fourth terraces. This suggests that another 7.7 m of the scarp resulted from the penultimate and preceding earthquakes that occurred after the formation of the third terrace. The amplitude of faulting for the penultimate event has been determined in the upper quarry section on the left bank of Kyngarga River, where the lowest horizon of a buried soil shows rupture and minimum vertical displacement of >0.7 m (McCalpin and Khromovskikh, 1995). The age of this event, estimated from four radiocarbon dates, is ranging from 6226 cal BC to 4808 cal BC years.

As for now, nine trenches have been made within the Arshan palaeoseismic structure, in which the humic-rich and carbon-bearing samples have been collected from buried soils for radiocarbon dating, and the nature of tectonic deformations has been studied to determine kinematics of displacements. The two quarry trench wall sections and the first 13 radiocarbon dates are presented in McCalpin and Khromovskikh (1995). This study also provides the preliminary conclusions on the age of three Holocene earthquakes and the earthquake recurrence on the latitudinal segment of the Arshan structure.

Some excavations have been made in the western segment of the Arshan structure to define parameters of paleoearthquakes and trends of amplitude variations along the strike of dislocations. The mouth of the valley of the east tributary of the Bugutai River, as well as the erosion pattern to the west of it, display some strike-slip dislocations with low-amplitude left-lateral westward motions.

3. Palaeoseismic interpretation of trench cross-sections

The A-3 trench is located in the east side of the valley of a intermittent stream, in its depositional part, 7 m above the top surface of the alluvial fan (the mouth of the creek) (Fig. 3). The trench wall exhibits a short segment of fault trending NE that links two latitudinal en-echelons of scarps of the normal fault of W–E trending. The section on the upthrown block contains talus-debris flow sand–rubble deposits, including small and large boulders and alluvial gravel or pebble layers. The trench wall clearly shows the fault plane and several antithetic ruptures extending upward radially from the foot of the fault (Fig. 7). The boulder layer (unit A) overlying the pebble bed (unit B) is broken at the downthrown side into blocks whose boundaries and, sometimes, inner parts are viewed as the seat of intrusion of sandy and fine-grained rubbly talus accumulated during the post-seismic period. All rupture-separated blocks show partial mixing in talus materials and some rubble and small boulders occurring along the block boundaries. At the bottom of the section, the normal fault is marked by a relatively small plate-shaped boulder substrate, which follows the fault plane that allowed determination of fault dip and strike: strike azimuth 52° with a steep (approximately 80°) dip towards the southwest.

The main benchmark for determining the amplitude of the fault is the stratigraphically consistent sequence, which can be correlated across the fault plane. The sequence is represented by boulder gravel (unit A), sand-pebble alluvial deposits (units B and C) overlain with another boulder gravel (unit D). The vertical

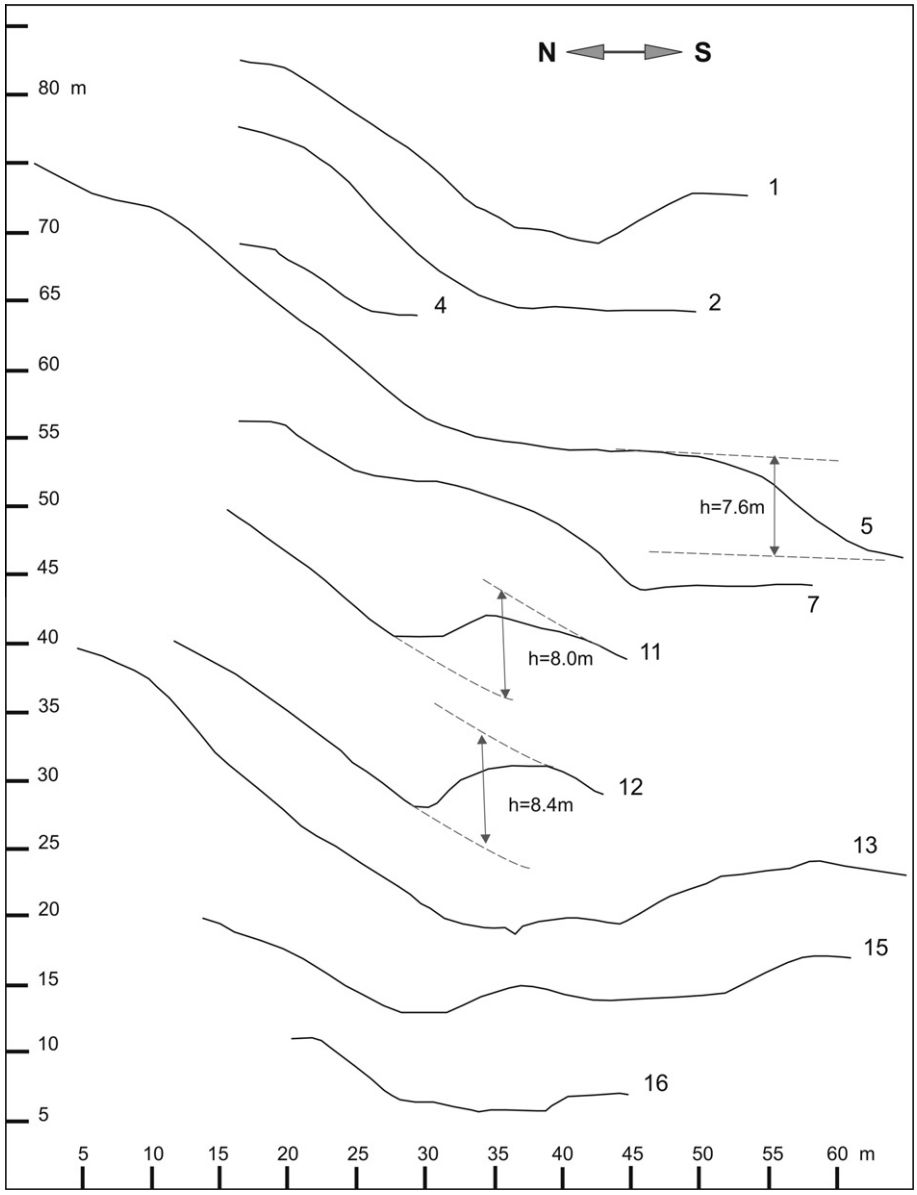

Fig. 4. Cross-section profiles through the seismogenic scarp of the Arshan structure. The numbers correspond to individual profiles. Profiles 11 and 12, which were made across the reverse-fault scarp, are supplemented with data on total amplitudes of vertical displacements.

displacement of these units along the fault is 0.9 m, which is 0.4 m less than that found on the second terrace on the west side of Kyngarga River. Deconsolidation of rubble and small boulder rocks on the downthrown side of the fault involved the development of cavities along the fault plane, which resulted in mixing between the rocks of a former hanging wall surface and the overlying sediments of a colluvial wedge (unit E). The post-seismic period was associated with accumulation of a brown sandy loam stratum, high (>50%) in coarse-grained material (gruss, rubble and small boulders) with interlayered humus-bearing black loams (unit F). The present-day surface of the steady-state slope serves as a basis for the development of a relatively thick (up to 20 cm) soil.

A sample was taken for radiocarbon dating from the faulted humic horizon (unit C4) in the footwall of trench A-3 to determine the age of the fault movement. Laboratory results showed that the soil horizon including unburnt carbon-containing ash was buried no earlier than 551–242 cal BC years (sample NUTA-3072, laboratory age 2340 ± 80, Table 2). This date provides a poorly-limiting maximum age for the paleoseismic event identified for this exposure, because an additional 1-m of thick diluvial-proluvium deposits (unit A) was deposited after this date, but before the paleoseismic event. A date of 695 ± 35 ^{14}C yrs from organics (unit F2) high over the colluvial wedge likewise provides a poorly-limiting minimum age for the paleoseismic event.

Trench A-1 was excavated at the top of an alluvial fan deposit 7 m away from Trench A-3 to estimate the rate for debris flow entrainment along the erosion valley (the wall of A-3 trench is on the erosion valley side, A-1 is a trench in alluvial fan deposit). Trench A-1 exposed complex deposits composed of alternating 0.2–0.3 m thick sub-horizontal layers of small and medium-sized rubble, randomly deposited coarse debris and boulders, and inclined horizons of humus-bearing black loams. As expected, such sequence shows periodic changes in the conditions of the steady development of the slope with the formation of thick layers of soil and abrupt sediments delivery. A gentle slope alluvial fan and abundant melt waters flowing from the valley contribute to rapid development of thick soil horizons. One of the humus-bearing loams at a depth of 2 m that is 0.2–0.3 m thick could have been

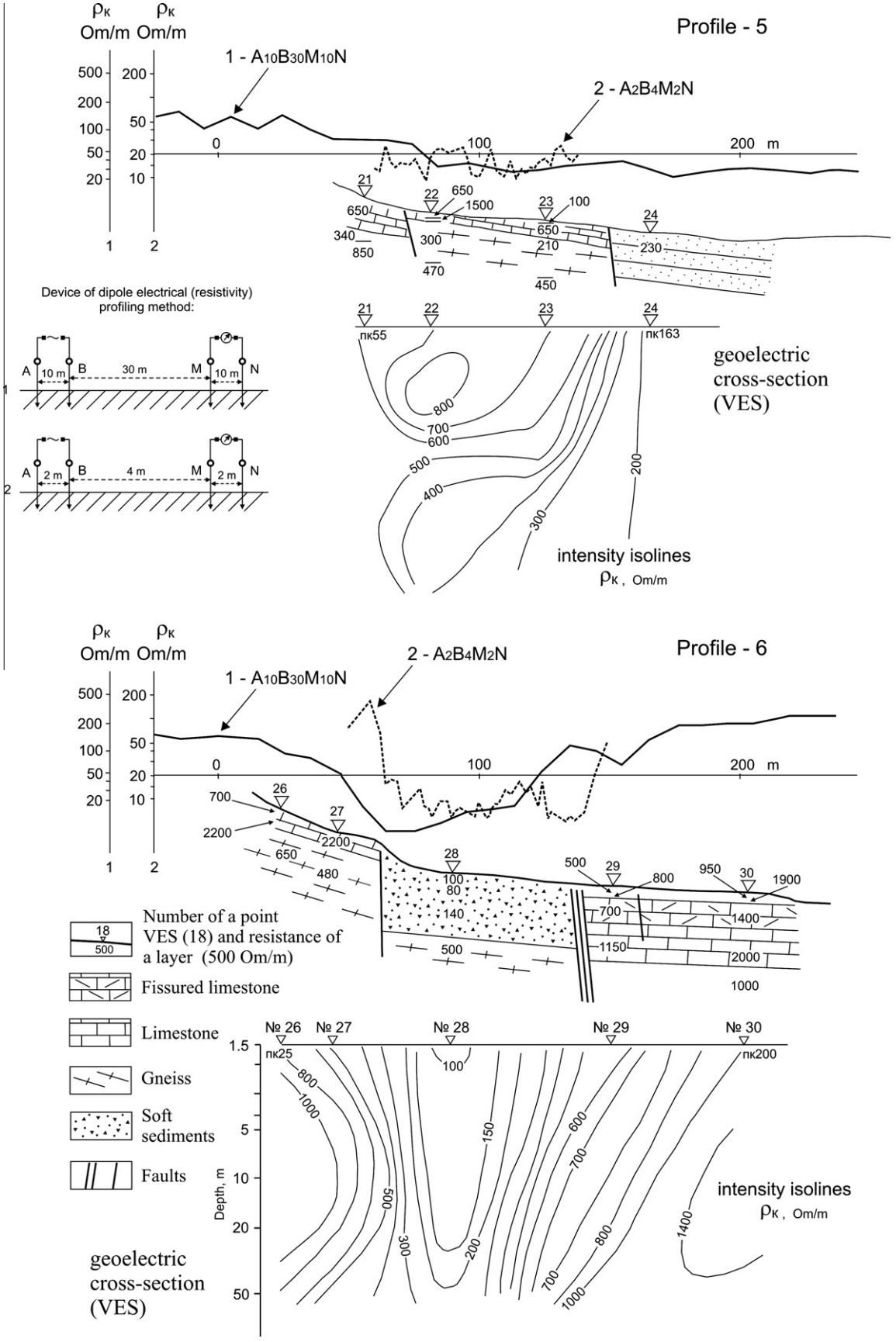

Fig. 5. Interpretation and results of geoelectric and vertical electric sounding survey (ВЭЗ) along profile PR-6. The locations of the profiles acquired during the detailed structural–geophysical research of the Arshan structure are represented in Fig. 3 (the general diagram).

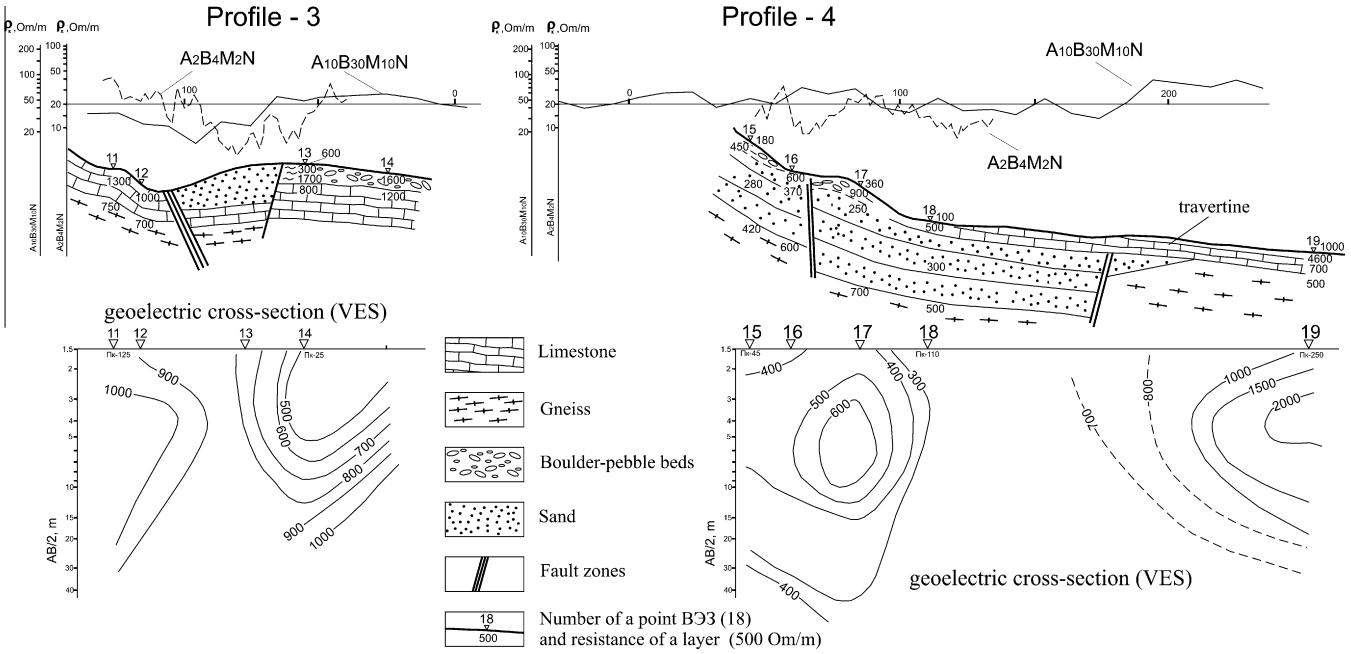

Fig. 6. Profiles 3 and 4, the structural–geophysical research of the Arshan structure.

Table 1
Amplitude of faulting, age and height of terraces at the mouth of the Kyngarga River (based on Lukina (1989), and McCalpin and Khromovskikh (1995)).

Terrace	Terrace height (m)	Terrace age, thousands years BP	Amplitude of faulting (m)
1	3	<1; (10–23)	None
2	4.5	1–6.7; (23–55)	1.3
3	24	>6.7; (55–110)	9.1–9.5
4	28	(110–180)	9.1–9.5
5	33	(180–290)	9
6	47	(290–500)	–

Note: The third column contains terrace age based on both paleoseismological evidence and data from corresponding heights on major rivers in southeast Siberia obtained from the literature (in brackets).

buried 120–260 years ago (sample NUTA-3068). A more than 1.5 m-thick rubble–boulder stratum separating the buried and contemporary soil horizons accumulated over a relatively short period of time as the result of one or several episodes of debris flow sedimentation. The cross-section of Trench A-1 illustrates intensive erosion within the front scarp of the Tunka uplift, particularly associated with propagation of loose debris flow along the valleys cut by temporary streams.

Trench A-2 is located west of Trench A-3 on the east side of the Buhota River valley, at the bottom of a step-like mountainous slope on the sub-horizontal site with surface layer composed of alluvial deposits. The N–S-trending trench was excavated in August 1996. In 1997, its western wall was cleared and logged. The trench is more than 17 m long and 2 m deep on an average (Fig. 8). The trench revealed colluvial and alluvial deposits. The former are dominant at the trench bottom and near the slope; there are some voids between large boulders. Fig. 9 shows the right half of the western trench wall, complicated by seismogenic deformation in the middle part. The last event caused the surface deformation and formation of fissures filled by small-sized loose alluvial sediments with fragments of humus-bearing layers, because of which a spot-textured sand-loam layer (unit S), dipping steeply towards the south, became enclosed in rubble–boulder substrate (unit A). This unit is about 25 cm in thickness and more than 1 m long downdip. The local deconsolidation along with the subsequent redeposition of the surface layers and, perhaps, some downthrowing of the south side of the fault resulted in the formation of a small, 1.2 m wide and 0.5 m deep syncline just above this fissure. The syncline has a defined thin humus-bearing layer (unit E5). This layer is consistently overlain by the beds of alluvial loamy sand with small pebbles (unit F1–F5, a maximum of 0.47 m thick), accumulated prior to the seismic event. These deposits entirely fill the inner syncline, being somewhat washed out and overlain by a layer of sandy loam (unit G) showing persistent thickness throughout the section and underlying the present-day soil-vegetation system (unit H). The two last layers (units G and H, 0.35 m thick) do not bear any evidence of activity.

The lower age boundary of the paleoearthquake traced from Trench A-2 coincides with the age of the uppermost folded sediments filling the syncline (i.e., the top of unit F5). The upper age boundary is defined by the starting time of sedimentation of sandy loam material (unit G) underlying the present-day soil. Three samples were collected in the trench for ^{14}C dating. Sample COAH-3650 whose radiocarbon age is 3630 ± 45 years was taken from the lower thick humus-bearing loam (unit D) with a high content of burning-related charcoal. Sample COAH-3649 was taken from the upper thin humus layer (unit E5) at the site of increasing layer thickness bearing convincing evidence for ancient burning. The ^{14}C age of this sample is 1900 ± 30 years. Sample ГИН-9611 (2320 ± 40 ^{14}C yr) was taken from the opposite wall of the trench, at a 2-m depth of humus-bearing loam (similar to that at COAH-3650 sampling site).

In order to obtain a more precise age for the deformation features revealed in Trench A-2, we calculated the rate of sedimentation. The maximum age of the deformation event is the age of the top of unit F5. The age of this stratigraphic level was determined by estimating the time required to deposit the 0.47 m of units F1 through F5, and then subtracting that time from the age of dated unit E5. We first calculated sedimentation rate between dated units C and E5, by dividing the maximum thickness of sediments between them (0.88 m) by their age difference (1992[=1926 + 66] – 2184[=2047 + 137] cal years) (see Table 2). This yields a maximum sedimentation rate of 0.40 (mm/cal year)

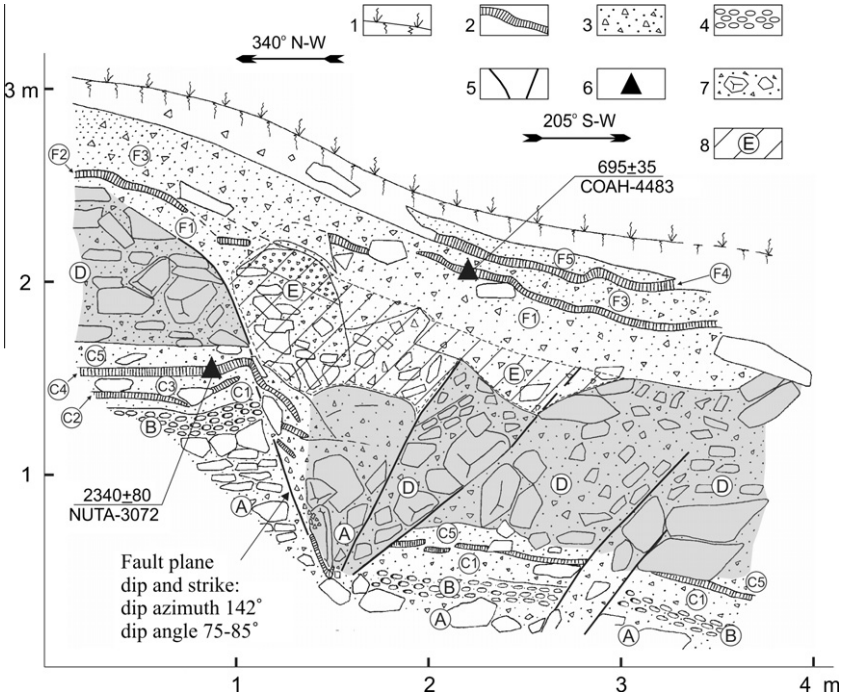

Fig. 7. The cross-section profile A-3 in the eastern side of a temporary stream, near the settlement of Arshan. The profile was documented by V.V. Ruzhich, O.P. Smekalin, and E.A. Deliansky in 1997 and 1999. Notations: 1 – present-day soil-vegetation cover; 2 – loam with a high humus content, black, occasionally brown with wood charcoal inclusions; 3 – mix of sandy loam and gruss, dark-brown with occasional inclusions of large gravel; 4 – fine-grained and medium-grained pebble bed with lightgrey sand; 5 – fractures exposed in the trench wall; 6 – radiocarbon sampling sites; 7 – light-gray sand–gravel–boulder mix.

Table 2
Radiocarbon dates of the Arshan structure.

Trench	Laboratory No.	Age ^{14}C	Sample type	Calendar age (BC), years	
1	2	3	4	Upper boundary	Lower boundary
A-2	COAH-3649	1900 ± 30	C	66 AD	137 AD
A-2	COAH-3650	3630 ± 45	C	2047 BC	1926 BC
A-2	ГИН-9611	2320 ± 40	S	420 BC	369 BC
A-1	NUTA-3068	210 ± 70	C	1633 AD	1952 AD
A-4	NUTA-3069	220 ± 110	C	1603 AD	1952 AD
A-3	COAH-4483	695 ± 35	C	1265 AD	1304 AD
A-3	NUTA-3072	2340 ± 80	C	551 BC	242 BC
A-5	ЛУ-2706	540 ± 60	S	1354 AD	1436 AD
A-5	4*	650 ± 40	S	1285 AD	1351 AD
A-5	5A*	600 ± 40	S	1324 AD	1394 AD
A-5	COAH	850 ± 20	C	1182 AD	1219 AD
A-5	ЛУ-2699	910 ± 70	S	1049 AD	1189 AD
A-5	1A*	1130 ± 50	C	859 AD	973 AD
A-5	ЛУ-2700	1440 ± 40	S	587 AD	640 AD
A-5	ЛУ-2707	2320 ± 40	S	420 BC	369 BC
A-5	ЛУ-2703	4900 ± 150	S	3916 BC	3535 BC
A-T-1	ЛУ-2710	1210 ± 70	S	729 AD	894AD
A-T-1	ЛУ-2709	6900 ± 420	C	6233 BC	5431 BC
A-6	ЛУ-2724	3590 ± 130	S	2116 BC	1762 BC
A-6	ЛУ-2718	3770 ± 50	S	2269 BC	2110 BC
A-6	ЛУ-2731	4210 ± 170	S	3006 BC	2539 BC
A-6	ЛУ-2734	5170 ± 150	S	4185 BC	3798 BC
A-6	ЛУ-2714	6890 ± 210	S	5985 BC	5620 BC
A-7	ЛУ-2729	6200 ± 150	C	5325 BC	4973 BC
A-7	ЛУ-2719	8420 ± 90	C	7564 BC	7389 BC
A-7	ЛУ-2713	8830 ± 170	C	8204 BC	7749 BC
A-7	ЛУ-2733	10470 ± 160	C	10632 BC	10198 BC
A-8	Poz-27775	835 ± 30	C	1188 AD	1235 AD
A-8	Poz-27774	1655 ± 35	C	356 AD	436 AD
A-8	Poz-27778	3595 ± 35	C	1991 BC	1909 BC
A-8	Poz-27777	4560 ± 40	C	3372 BC	3138 BC

Notes: Column 4 uses the following abbreviations: C – wood charcoal, S – buried soil, mostly humus-bearing loams. The calendar age of the sample were calculated using CALIB v.6.0 (Stuiver and Reimer, 1993).

[=880/2184] – 0.44 (mm/cal year) [=880/1992]. Then, we applied these sedimentation rates to 0.47 m-thickness of units F1–F5, which predicts that 1068–1175 cal years were required to deposit units F1 through F5. Thus, the lower chronological boundary of the

Fig. 8. Trench A-2, viewed from the side of the basin.

deformation event occurred 1068–1175 years after the age of dated unit E5 (66–137 cal AD), or roughly 700–900 years ago.

The upper chronological boundary of the paleoevent (its minimum age) could be roughly calculated by applying the undeformed layer thickness (0.35 m) to same sedimentation rate, yielding a minimum age of 795–875 years. This is an approximate or rough estimate though an appropriate set of statistical data may provide a more precise age determination based on sediment thickness and sedimentation rates within ^{14}C time intervals.

The multistage deformation traced from Trench A-2 suggests that if the bottom, thick humusbearing loam, prior to being underneath the overlying beds, showed deformation similar to or associated with the graben formation, then there would be an increase in thickness of sediments separating the humus beds deposited prior to and after the earthquake. In the same way, the steepness of the dip of the beds would be expected to increase from bottom to top. Since none of these features are found in the investigated section, we may suggest that the deformations described in Trench A-2 have been produced by a single seismic event. Medium-sized and large colluvial boulder deposits in the bottom section (see Fig. 9) could possibly be related to an earlier, undated seismic event.

Trench A-8 (Fig. 10) was excavated to determine the age and mechanism for a compensation structure at the junction of segments of the latitudinal and NE-trending faults. The trench, excavated in the transverse direction, crossed the reverse-fault scarp and axis of a narrow enclosed trough between this scarp and range slope. The trough is 350 m long, 5 m deep, and has an arch shape, with south-facing convex side and demonstrates slope-parallel westward uplift. Morphological features of this structure (see transverse profiles 11 and 12) bear evidence of reverse-fault style of motions. The exogenous origin of the structure is excluded.

Trench 8 was 9 m long with a depth of about 1.5 m within the uplifted side of the scarp, and up to 2.5 m were it crosses the fault scarp and trough (Fig. 11). The western wall of the trench was logged. The composition and radiocarbon age of the deposits exposed beneath the trough (right section) indicate that sandy loam strata have been accumulating in the trough for more than six thousand years in the closed basin.

The dam preventing runoff at the eastern tip of the trough is about 0.5 m heigh, and currently creates a closed depression a few meters wide and tens of meters long. The stratified unit (unit F) is as thick as 0.6–0.7 m as a whole. It is composed of intercalating sandy loams and sandy gruss, with the strata of dark-brown and black sandy loam and loam. They have a high content of humus and peat, the latter sometimes being as thick as 7 cm. The peat is distributed throughout almost the entire unit. The stratified unit reported herein reflects the interseismic depositional environment. The paleoearthquakes were associated with the uplift of piedmont slope and collapse of some overhanging-scarp tips down to the trough bottom (unit G), producing colluvial wedges composed of rock debris, gruss and sand bulk materials from both deluvial-cover deposits and weathered rocks. The crossection shows two colluvial wedges, the lower one (unit C1) immediately overlying weathered rocks in the bottom but being stratigraphically higher than the sharply unconformable sedimentary clays (unit E) that are indicative of shear deformations. These clays found in the

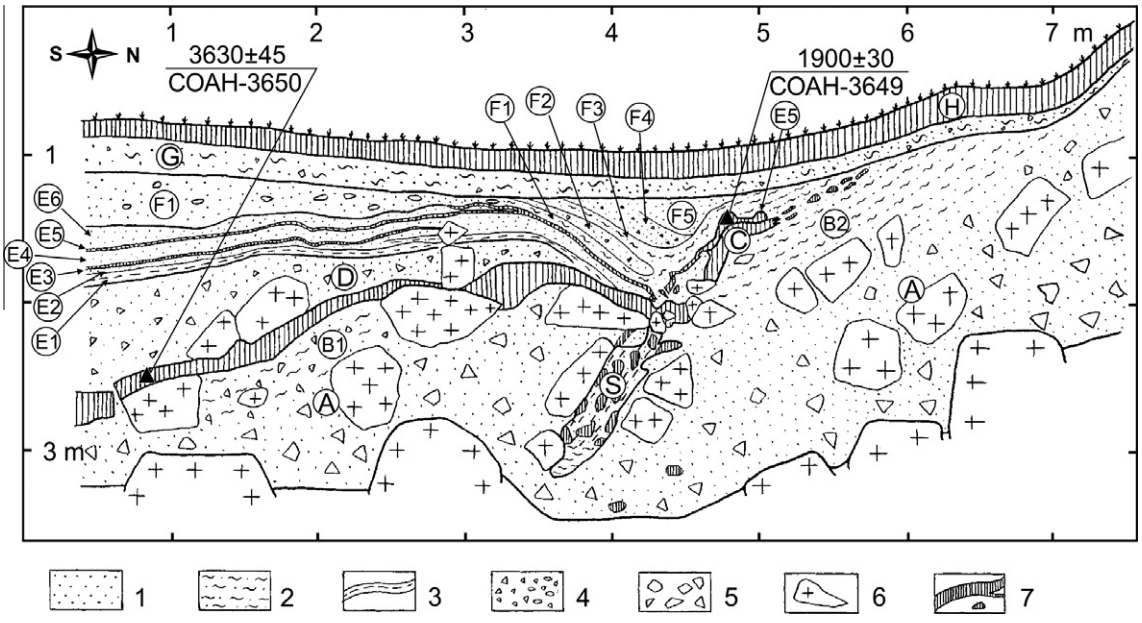

Fig. 9. Cross-section of the colluvial–deluvial deposits in the western wall of Trench A-2. Notations: 1 – sand, sandy loam; 2 – sandy-loam sediments; 3 – clayey-loam interlayers; 4 – gruss, gravel; 5 – fine-grained and medium-grained debris material; 6 – large individual rock fragments and boulders; 7 – present-day and buried soil layers and sandy-loam horizons with a high humus content and wood charcoal remnants.

Fig. 10. Trench A-8, viewed from the side of the Tunka ridge.

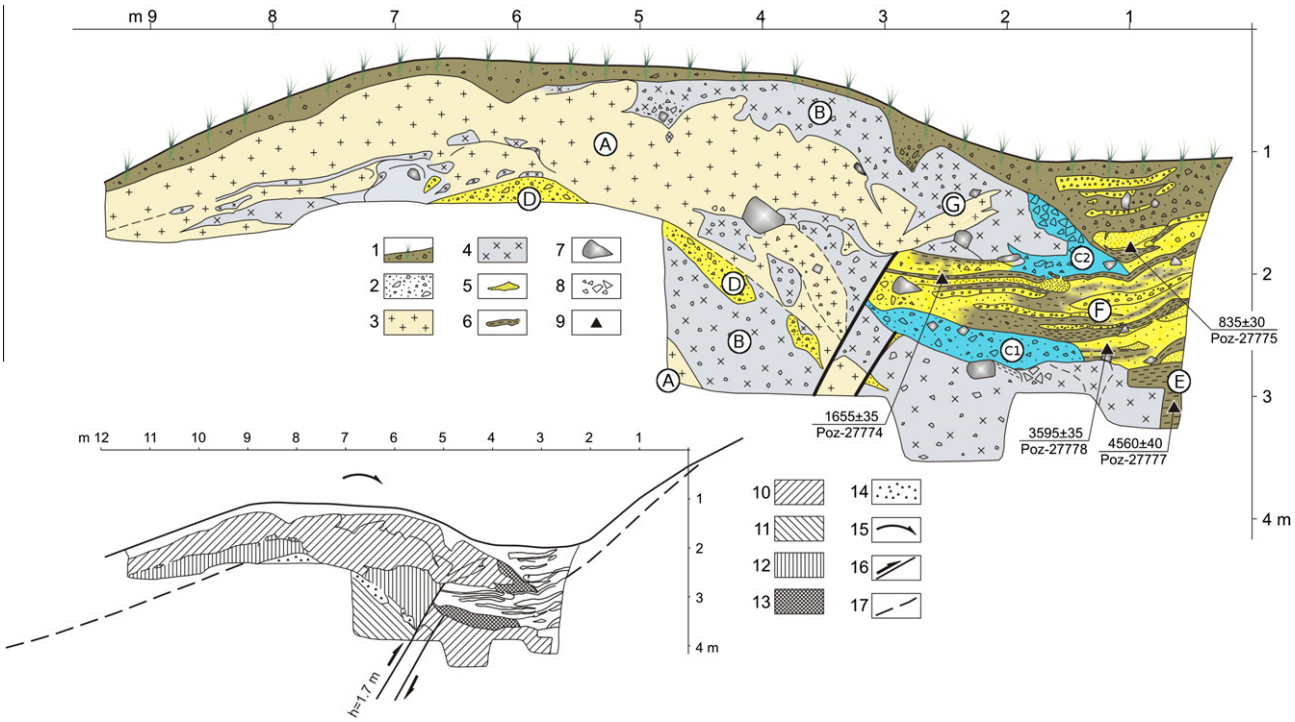

Fig. 11. Cross-section of the western wall of Trench A-8. Notations: 1 – modern topsoil (brown-black sand with admixtures of gravel–gruss rock debris material); 2 – soil material consisting of sand, rock debris and gruss; 3 – light yellow-red to greenishyellow loam with the same-color small-size debris and gruss inclusions; 4 – mass consisting of loam and medium-size debris material, black with a blue tint; 5 – largegrained and coarse-grained sand, sandy layers and lenses; 6 – loamy and clayey layers; 7 – some large-size debris and small-sized boulder rocks; 8 – debris accumulations; 9 – sites wherein peat samples are taken for radiocarbon dating analysis; 10 – thrust-related folds; 11 – folded layers without any horizontal displacement; 12 – transition zone; 13 – colluvial wedge deposits; 14 – washed drifts (sand, gruss, rock debris); 15 – thrust-related fold surface trend; 16 – reverse-fault planes; 17 – ground surface reconstruction for the penultimate paleoevent. (For interpretation of the references to color in this figure legend, the reader is referred to the web version of this article.)

lower right corner are unstratified and contain charcoals. The sample (Poz-27777) was taken there for radiocarbon dating to provide the lower age limit for the paleoevent associated with the lower colluvial wedge formation (unit C1).

The upper colluvial wedge (C2) divides the stratified unit into the parts of approximately equal thickness. The admixture of gruss and rock debris that composes the wedge is moved to the right through the lateral displacement of the strata in the uplifted piedmont slope. The central and left sections of the trench show an anticline in strata whose contacts parallel the ground surface. The folded strata are composed of two types of loamy sediments: yellowish-brown loams (unit A), with some rock debris inclusions, and dark-gray (to bluish-black) loams (unit B), wherein the debris are predominantly mid-size. Both cases involve weathered disintegrated rocks that originated respectively from granite materials (unit A) and marmorized limestones (unit B).

A strong interface between the strata has been revealed on short segments at the uplifted side of the scarp only. Vertical stratification sequence in these two sedimentary beds recurs twice in the section, with "granite" bed being overlain each time by "marmorized limestones". The interface extending along the conjugate section exhibits intercalations, lenses and some inclusions of washed gruss and coarse-grained sand (*dr* beds, unit D) that might have been accumulated on the ground surface, on the top of the "limestones" bed. The same interface attracts intercalation and wedging segments of thin beds in the left section, and a zone of interbedded fragments that was probably formed by hummocks resulted from the lateral displacement of the top bench. This zone is cut off from sedimentary deposits on the right side by the steeply dipping reverse fault with a strike-slip component.

The fault plane exposed in the trench wall represents the orderly sequence of stratified debris concentrated along two linear stripes, each of which are about 15 cm wide. The fault plane is distinctly traced both in the western and eastern trench walls that allowed determining its basic parameters: strike azimuth of 260°, dip angle of 62° towards the basin. The deformation behavior discovered by the trench excavation gives evidence of multiple impulsive motions associated with the uplift on the fault side of the piedmont slope and formation of anticline.

Four samples have been taken from the trench for radiocarbon dating. These are black and brown humus loams with a high charcoal content. The dating of samples Poz-27778 and Poz-27777 determines respectively the upper (1991–1909 cal yr BC) and lower (3372–3138 cal yr BC) limits for the lower colluvial-wedge formation time, as do samples Poz-27775 (1188–1235 cal yr AD) and Poz-27774 (356–436 cal yr AD) with regard to the upper colluvial wedge and associated last paleoearthquake.

The dislocation that is revealed in Trench A-8 between the fault segments, showing different types of motion, does not make any fault-segment extension suggesting mechanism of compensatory development. The left-lateral displacements along the fault west from the site give rise to the eastward motion of the downthrown side of the fault and to the pressure that it exerts on the part of a WNW-trending slope, which provides a link between two en-echelon folds within the Tunka fault zone. The occurrence of the left-lateral displacements along the western fault section and the lack of displacements of this type along the latitudinal en-echelon fold, which adjoins the structure on the east, led to the formation of a wide N–S trending subsidence trough with smooth topography through extension of the downthrown side of the fault. The trough mouth is therewith at the base of the reverse scarp on the piedmont side of the fault.

4. The age of the Arshan palaeoearthquakes

During the 1991 field studies, 13 radiocarbon samples for 14C dating were collected from four excavations: the upper (A-6) and lower (A-7) gravel quarry exposures showing a seismogenic scarp at the east boundary of the Kyngarga River alluvial fan; a small trench (A-5) in the trough at the base of the scarp on the 3rd terrace; and a small excavation on the surface of the 1st terrace (AT-1). The radiocarbon dates, excavation documentation analysis, and the correlation between the terrace and terrace-dislocating fault scarp formation processes returned ages of three Holocene earthquakes (McCalpin and Khromovskikh, 1995).

The age of the last paleoearthquake (420 cal yr BC–894 cal yr AD) was estimated from radiocarbon dating of the samples from AT-1, A-5, and A-6. The accompanying deformations were revealed in A-3, A-2, and A-8. The layers uncovered therewith were deformed during the last paleoearthquake or overlain by colluvial wedge sediments. In none of these cases was there a discrepancy

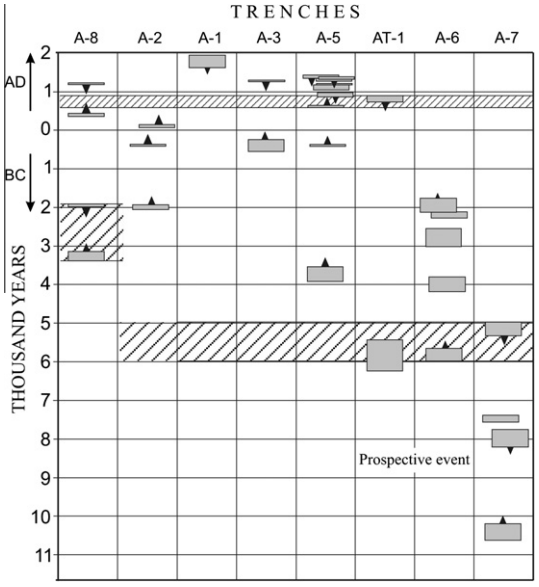

Fig. 12. Correlation of radiocarbon (calibrated) ages of deformation events on the Arshan seismic structure.

with earlier results of the paleoearthquake dating (Fig. 12). Moreover, the age constraints for the lower bound of the paleoearthquake occurrence, dates of the layers uncovered in trenches A-8 and A-2 and the ages of additional samples from Trench A-5 severely constrained the time of occurrence of the last earthquake raising the lower bound from 420 cal yr BC to 587 cal yr AD. An important outcome of the above work is the along-fault tracing the deformations resulting from ground motions produced by a single paleoearthquake.

The excavations west from the Kyngarga River have not revealed any earlier paleoevents considered in McCalpin and Khromovskikh (1995). On the other hand, all deformations observed in the trench suggest earthquake recurrence. The seismic event recognition became possible with dislocation zone exposed in the quarry (Fig. 3) extending over several tens of meters (the total height of the fault zone exposure is about 30 m). Therefore, the exploration of the penultimate (5985–4973 cal yr BC) and earlier (e.g. 10,632–7389 cal yr BC) paleoevents requires a special methodology and considerable expenses.

Trench A-8 is the only one tracing and dating the deformations of the paleoearthquake occurred within the range from 3372 cal yr BC to 1909 cal yr BC. Although the type of motion for deformations in Trench A-8 is almost exactly the opposite of that in the other trenches, it supports the fact that all these motions may occur either simultaneously or alternately.

5. Conclusions

The recognition of a new event on the western flank of the Arshan structure, as well as imposing age constraints on the last paleoearthquake, introduce some significant changes in the earlier estimate of surface-rupturing earthquake recurrence. Paleoevents occurred there at least four times over the last 13,000 years, once every 3000 years on the average. The minimum recurrence interval between two events is 2500–4270 years. For the last three events, it ranges from 2780 to 3440 years. Compared to the recurrence interval of 2976–6843 years reported in McCalpin and Khromovskikh (1995), our estimate of the maximum recurrence interval appears to be two times shorter.

The individual amplitudes of faulting obtained for various sites of the structure demonstrate its insignificant but with consistent

decrease in size west from the Kyngarga River. The reverse fault extending for about 350 m at the western flank of the structure shows single-event displacements of 1.7 m and the total displacement up to 4.6 m. When coupled with interpretative information on the section across Trench A-8 this will allow us to suggest the occurrence of three paleoevents resulted in formation of the crest of the reverse-fault structure. The recurrence interval for deformations, revealed in Trench A-8, and the age of deformations in the lower quarry exposure imply that the third event, initiated the reverse fault scarp growth on the Buhota-Bugutai interfluve slope, could be contemporaneous with the second event in the Kyngarga River deposits. That is to say, the deformations in question were produced by the same paleoearthquake whose age range is 5985–4973 cal yr BC. In this connection and in the context of reverse faults caused by the left-lateral movements along the western flank of the structure, it is pertinent to note that 8-m displacements on the east side of Bugutai River are about 7000–8000 years old. Since no other evidence was found for Holocene strike-slip or reverse fault movements within the Arshan structure, the studied crest of reverse-fault structure may be considered as a unique local anomaly, and the associated strike-slip motions – as an ‘‘outburst of strike-slip activity’’ against the background of long-term normal faulting.

Acknowledgments

The authors thank A.V. Chipizubov and T.V. Leshkevich, who collaborated in this research. The project has been made possible through the financial support of the Russian Foundation for Basic Research (Grant # 11-05-00666, 12-05-00544, 12-05-98028, 11-05-00075, 12-05-33003), the Baikal Archaeology Project, Social Sciences and Humanities Research Council of Canada and Research-Educational Center ‘‘Baikal‘‘.

References

Arzhannikova, A.V., Melnikova, V.I., Radziminovich, N.A., 2007. Late Quaternary and current deformation in the western Tunka system of basins: evidence from structural geomorphology and seismology. Russian Geology and Geophysics 48 (4), 305–311.

Chipizubov, A.V., Smekalin, O.P., Semenov, R.M., 2003. Fault scarp and prehistoric earthquakes in the Tunka fault (southwestern Baikal region). Russian Geology and Geophysics 44 (6), 587–602.

Florensov, N.A., 1960. Mesozoic and Cenozoic depressions of the Cis-Baikal region. Moscow-Leningrad, 258 p. (in Russian).

Florensov, N.A., 1969. Rifts of the Baikal mountain region. Tectonophysics 8, 443–456.

Logachev, N.A., 2003. History and geodynamic of the Baikal Rift. Russian Geology and Geophysics 44 (5), 391–406.

Lukina, N.B., 1989. Quaternary movements along the fissures of the southwest flange of the Baikal rift zone. Geotektonika 2, 89–100 (in Russian).

Mccalpin, J.P., 2005. Late Quaternary activity of the Pajarito fault, Rio Grande rift of northern New Mexico, USA. Tectonophysics 408, 213–236.

Mccalpin, J.P., Khromovskikh, V.S., 1995. Holocene paleoseismicity of the Tunka fault, Baikal rift, Russia. Tectonics 14 (3), 594–605.

San'kov, V.A., Chipizubov, A.V., Lukhnev, A.V., Smekalin, O.P., Miroshnichenko, A.I., Calais, E., Devercher, J., 2004. Assessment of a large earthquake risk in the zone of Main Sayan fault using GPS geodesy and paleoseismology. Russian Geology and Geophysics 45 (11), 1369–1376.

Shchetnikov, A.A., 2009. The manifestation of a global mechanism of orogenesis in the Baikal rift zone (using the Tunka rift as an example). Geography and Natural Resources 29, 226–229.

Shchetnikov, A.A., White, D., Filinov, I.A., Rutter, N., 2012. Late Quaternary geology of the Tunka rift basin (Lake Baikal region), Russia. Journal of Asian Earth Sciences 46, 195–208.

Solonenko, V.P., 1975. Seismotectonics and seismicity of a southeast part of East Sayan ridge. Novosibirsk, Nauka 134 p. (in Russian).

Solonenko, V.P., Khromovskikh, V.S., Zhilkin, V.M., Golenetskij, S.I., Kurushin, R.A., 1971. Some Seismotectonics and engineering-seismogeological aspects of a jolting problem at earthquakes. In: Solonenko, V.P. (Ed.), Studying of Seismic Danger. Tashkent FAN, pp. 84–118 (in Russian).

Stuiver, M., Reimer, P.J., 1993. Extended 14C data base and revised CALIB 3.0 14C age calibration program. Radiocarbon 35 (2), 215–230.

Zorin, Y.A., 1972. Neotectonics and isostasy of the Baikal rift zone and adjacent territories, Moscow, Nauka 167 p. (in Russian).